

## Optical-Model Analysis of Elastic Scattering of Protons on Carbon at Intermediate Energies\*

J. S. NODVIK

*University of Southern California, Los Angeles, California*

AND

C. B. DUKE

*Princeton University, Princeton, New Jersey*

AND

M. A. MELKANOFF

*University of California, Los Angeles, California*

(Received September 8, 1961)

Differential cross sections and polarizations for the elastic scattering of protons by carbon at energies between 7 and 20 Mev have been analyzed according to the diffuse-surface optical model of the nucleus. The model parameters were varied systematically, the best fits to the experimental data being determined by a method of least squares. Various forms of the absorptive part of the potential were investigated, although the main part of the analysis was carried out with a surface-plus-volume absorption potential. It was found that the model could not account satisfactorily for the data below about 12 Mev, and the presentation of results is limited to the region  $11.85 \text{ Mev} \leq E_{\text{lab}} \leq 19.4 \text{ Mev}$ . Excellent fits can be obtained over the latter region with generally reasonable values of the model parameters, although some features of their behavior as a function of energy remain to be explained. The most striking feature of the results is the thin absorptive shell and small volume absorption which characterizes the potential. Although the predicted reaction cross sections appear generally too low, the experimental data are not sufficiently precise to warrant drawing a definite conclusion.

### I. INTRODUCTION

THE nuclear optical model has been shown to be quite successful in accounting for the angular distributions and polarizations of protons elastically scattered by intermediate and heavy nuclei.<sup>1</sup> Attempts to apply the model to light nuclei, however, have not been nearly so successful. This apparent limitation has been accepted as inherent in the model: the wide level spacing found in light nuclei presumably invalidates the usual low-energy justifications of the model. Before finally accepting this conclusion, however, it was decided to undertake a systematic analysis of a typical light nucleus. This analysis was further prompted by the possible need for accurate optical-model wave functions for use in distorted wave calculations of inelastic scattering. Carbon was selected as the target nucleus because of the availability of a large amount of accurate experimental data at small energy intervals over a sizeable range.

As a result of an exhaustive analysis with various optical-model potentials over a wide range of parameters, it was indeed found that excellent fits can be obtained to the experimental data on the elastic scattering of protons on carbon from 12 to 20 Mev. The

parameters characterizing the potential are generally reasonable, although their behavior as a function of energy sometimes exhibits a more detailed structure than might be expected *a priori*.

### II. EXPERIMENTAL DATA

The primary consideration in selecting the data used in the present analysis was the availability of differential elastic scattering cross sections at small energy intervals. This stipulation restricted the analysis to the energy region between 6 and 20 Mev. However, in the course of the analysis, it was found that the model could not satisfactorily account for the data below about 12 Mev, and the presentation of results is limited to the region  $11.85 \text{ Mev} \leq E_{\text{lab}} \leq 19.4 \text{ Mev}$ . The experimental data,<sup>2-9</sup> which were used in the analysis for  $11.85 \leq E_{\text{lab}} \leq 19.4 \text{ Mev}$ , are presented in Table I.<sup>10</sup>

<sup>2</sup> H. E. Conzett (private communication); see also: H. C. Shaw, H. E. Conzett R. J. Slobodrian, and R. G. Summers-Gill, *Bull. Am. Phys. Soc.* **1**, 253 (1956).

<sup>3</sup> Y. Nagahara, *J. Phys. Soc. Japan* **16**, 133 (1961).

<sup>4</sup> R. W. Peelle, *Phys. Rev.* **105**, 1311 (1957).

<sup>5</sup> W. Daehnick and R. Sherr (private communication); see also: W. Daehnick, M. Garrell, R. Wood, and R. Sherr, *Bull. Am. Phys. Soc.* **6**, 25 (1961).

<sup>6</sup> I. E. Dayton and G. Schrank, *Phys. Rev.* **101**, 1358 (1956).

<sup>7</sup> L. Rosen and L. Stewart (private communication); see also: L. Rosen, J. E. Brolley, and L. Stewart, *Phys. Rev.* **121**, 1423 (1961).

<sup>8</sup> S. Yamabe, M. Kondo, S. Kato, T. Yamazaki, and J. Ruan, *J. Phys. Soc. Japan* **15**, 2154 (1961).

<sup>9</sup> K. W. Brockman, *Phys. Rev.* **110**, 163 (1958).

<sup>10</sup> In the low-energy analysis, cross-section data at approximately fifteen energies between 6.74 and 11.51 Mev (reference 3) were analyzed in conjunction with polarization data at 8 Mev (reference 7).

\* This work was supported in part by the U. S. Atomic Energy Commission, the National Science Foundation, and the Air Force Office of Scientific Research.

<sup>1</sup> See, for example: M. A. Melkanoff, J. S. Nodvik, D. S. Saxon, and R. D. Woods, *Phys. Rev.* **106**, 793 (1957); A. E. Glassgold, W. B. Cheston, M. L. Stein, S. B. Schuldt, and G. W. Erickson, *ibid.* **106**, 1207 (1957); A. E. Glassgold and P. J. Kellogg, *ibid.* **107**, 1372 (1957); F. Bjorkland, *Proceedings of the International Conference on the Nuclear Optical Model, Florida State University Studies No. 32* (Florida State University, Tallahassee, 1959).

TABLE I. Experimental data on elastic  $p$ -C scattering used in the analysis.

Laboratory	Reference	$E_{lab}$ (Mev)
Differential elastic scattering cross sections		
Berkeley	2	11.85
Tokyo	3	12.07, 12.25, 12.43, 12.67, 13.06, 13.21, 13.35, 13.48, 13.64, 13.92, 14.36, 14.94, 15.11, 15.37, 15.50, 15.66, 15.79, 15.92
Princeton	4	14.0, 14.7, 15.2, 15.6, 16.2, 16.7, 17.4, 17.8, 18.9, 19.4
Princeton	5	14.0, 14.7, 15.2, 15.6, 16.2, 16.7, 17.4, 17.8, 18.9
Princeton	6	18.4
Polarizations		
Los Alamos	7	11.5
Osaka	8	14, 16
Princeton	9	17.8

The method for determining the best fit to a set of data is based upon a  $\chi^2$  test, to be described below, which requires the assignment of an experimental error to every point. Whenever available, the errors were taken to be those quoted for the various experiments. Such was uniformly the case except for the Tokyo cross sections,<sup>11</sup> for which an error of 3% was assumed at each point, and for the Princeton cross sections at 19.4 Mev.

In the analyses of the Princeton differential cross sections (except at 19.4 and 18.4 Mev), Peelle's data<sup>4</sup> at the forward angles were combined with the data of Sherr *et al.*<sup>5</sup> at the back angles. At 18.4 Mev, the data of Dayton and Schrank<sup>6</sup> were used exclusively as were Peelle's data at 19.4 Mev. For the sake of consistency, the 19.4 Mev data were weighted in a manner identical to that used with the Peelle-Sherr combination.

Polarization data were available at only four energies as indicated in Table I. Since the inclusion of such data in the analysis is effective in fixing the spin-orbit strength, it was decided to associate one of these four polarizations<sup>7</sup> with each energy at which differential cross sections were analyzed. Therefore, the polarization data at 11.5 Mev were used over the range 11.85 Mev  $\leq E_{lab} \leq 13$  Mev, the 14 Mev data over the range 13 Mev  $< E_{lab} < 15$  Mev, the 16 Mev data over the range 15 Mev  $< E_{lab} < 17.4$  Mev, and the 17.8 Mev data over the range 17.4 Mev  $\leq E_{lab} \leq 19.4$  Mev. This procedure is based on the assumption that the polarization varies slowly with energy. Although this assumption is probably valid for most of the energy range investigated, recent measurements<sup>12</sup> indicate a rapid variation of the polarization in the 17-18 Mev region.

<sup>11</sup> This data was originally obtained as a private communication and has since been published in expanded form (see reference 3). In this publication, the author assigns a constant percentage error to each point at a fixed energy. This percentage varies from 2.5% to 3% depending upon the energy considered.

<sup>12</sup> E. Boschitz (private communication).

### III. INVESTIGATION OF VARIOUS OPTICAL-MODEL POTENTIALS

The optical-model potentials investigated during the course of the analysis are all of the form

$$V_{Opt} = V_{CN} + V_{SO} + V_{Coul}, \quad (1)$$

where  $V_{CN}$  and  $V_{SO}$  are, respectively, the (complex) central nuclear and spin-orbit potentials, and the Coulomb potential,  $V_{Coul}$ , is that corresponding to a uniformly charged sphere of radius  $R$ .<sup>1</sup> The real part of  $V_{CN}$  is given by

$$\text{Re}(V_{CN}) = -Vf(r), \quad (2)$$

where

$$f(r) = [1 + \exp(r-R)/a]^{-1}, \quad (3)$$

and  $R = R_0A^{1/3}$ . The spin-orbit potential is given by

$$V_{SO} = -\left(\frac{\hbar}{m_\pi c}\right)^2 (V_S + iW_S) \left(\frac{1}{r}\right) \frac{df}{dr} \cdot \mathbf{l}. \quad (4)$$

Four different forms of the imaginary part of the central nuclear potential were investigated.

(1) Volume absorption

$$\text{Im}(V_{CN}) = -Wf(r). \quad (5)$$

(2) Volume plus derivative surface absorption

$$\text{Im}(V_{CN}) = -Wf(r) + 4aW_1 df/dr. \quad (6)$$

(3) Gaussian surface absorption

$$\text{Im}(V_{CN}) = -W_1 \exp[-(r-R)^2/b^2]. \quad (7)$$

(4) Surface-plus-volume absorption

$$\text{Im}(V_{CN}) = -W_1 \exp[-(r-R)^2/b^2] - W[1 + \exp(r-R)/0.69b]^{-1}. \quad (8)$$

The factor 0.69 in Eq. (8) arises from the requirement that the volume term fall from 90% to 10% over that interval in which the Gaussian surface term exceeds 10% of its maximum value. Such a characterization of the absorption avoids the introduction of an extra parameter.

Each of the potentials listed above was investigated in turn. The volume absorption potential, Eq. (5), proved completely unsatisfactory in accounting for the angular distributions at the back angles and was discarded in all further investigations. The potential characterized by volume plus derivative surface absorption, Eq. (6), was investigated next. Although reasonable fits were obtained at 17.8 Mev, those at the other energies were less satisfactory. A preliminary analysis with the potential characterized by Gaussian surface absorption, Eq. (7), yielded considerable improvement and it was decided to generalize it by adding a volume absorption term, Eq. (8). The resulting surface-plus-volume absorption potential, characterized by the eight parameters  $V$ ,  $W$ ,  $W_1$ ,  $V_S$ ,  $W_S$ ,  $R_0$ ,  $a$ , and  $b$ , was used exclusively in subsequent analyses. During the course of the investigation it was found that

a small value of  $W_S$  was indicated and thereafter this parameter was set equal to zero. *All further mention of parameters refers to the surface-plus-volume absorption potential with  $W_S=0$ .*

#### IV. METHOD OF ANALYSIS

The cross sections and polarizations were calculated in the usual way<sup>13</sup> on the IBM 709 and 7090 computers at UCLA. The optimum fit to the experimental data is defined as the one which minimizes the quantity  $\chi^2$  defined by

$$\chi^2 = \chi_\sigma^2 + \chi_P^2, \quad (9)$$

where

$$\chi_\sigma^2 = \sum_i \left[ \frac{\sigma^{\text{th}}(\theta_i) - \sigma^{\text{ex}}(\theta_i)}{\Delta\sigma^{\text{ex}}(\theta_i)} \right]^2, \quad (10)$$

and

$$\chi_P^2 = \sum_i \left[ \frac{P^{\text{th}}(\theta_i) - P^{\text{ex}}(\theta_i)}{\Delta P^{\text{ex}}(\theta_i)} \right]^2. \quad (11)$$

It should be noted that  $\chi^2$  thus defined does not include any consideration of the reaction cross section. For a given set of experimental data, the quantity  $\chi^2$  is a function of the  $N$  optical-model parameters which can be considered to define an  $N$ -dimensional space.

The optimum fits were obtained by an automatic search program which minimizes  $\chi^2$  by simultaneous variation of certain of the parameters. A local quadratic approximation to the actual  $\chi^2$  surface is constructed in the neighborhood of a given point in the  $N$ -parameter space. Using this approximation the parameters are changed in such a way as to advance along the gradient in the direction of decreasing  $\chi^2$ . When the parameters have departed sufficiently from their initial values, the original approximation becomes inadequate and a new quadratic surface must be constructed. This process is repeated until  $\chi^2$  reaches a local minimum.

Although the above procedure leads to a minimum value of  $\chi^2$ , this minimum may not be particularly significant if the surrounding  $\chi^2$  surface is flat, i.e., if a large change in some of the parameters results only in a small change in  $\chi^2$ , as in the case of the well-known  $V-R_0$  ambiguity. In general, the extent to which the parameters are determined may be ascertained by investigating the nature of the  $\chi^2$  surface. Such an investigation was carried out to a limited extent by fixing a chosen subset of parameters, referred to as grid parameters, during any given search. A sequence of separate searches was then carried out in such a way that the values of the grid parameters mapped out a selected region of the parameter space.

Before presenting the results of the analysis, the approach used in investigating the parameter space will be described in more detail. Past experience had indicated the existence of a  $V-R_0$  ambiguity; similar

ambiguities were observed among the absorption parameters  $b$ ,  $W$ , and  $W_1$ , which, in addition, appear to be strongly coupled to  $R_0$ . In order to cope with the above difficulties, it was found expedient to select  $b$ ,  $W$ , and  $R_0$  as the grid parameters.

After a preliminary investigation to determine the general region of the grid parameter space in which acceptable results could be expected, the following grid was constructed:  $R_0=1.1, 1.2, 1.3$  f;  $W=0, 2, 4$  Mev; and  $b=0.25, 0.50, 0.75, 1.00, 1.25$  f. This grid was extended whenever the region of minimum  $\chi^2$  fell close to its initial boundaries, and a finer mesh was used in a number of cases. A similar but less extensive grid was also investigated for the radius parameter  $R_0=1.25$  f. At each grid point a search was carried out over the remainder of the  $N$ -parameter space yielding a set of parameters which minimizes  $\chi^2$  at that grid point. The optimum fit at a given energy was obtained with that set of parameters corresponding to the lowest of these minimal  $\chi^2$  obtained at the various grid points. An examination of the optimum fit parameters revealed that they did not vary systematically over certain energy regions. Moreover, systematic behavior as a function of energy could be achieved only by deviating from the optimum fit parameters. The value of  $\chi^2$  can be used as a quantitative measure of the extent of such deviations.

The significance of relative values of  $\chi_\sigma^2$  and  $\chi_P^2$  in terms of visual fits to the experimental data is illustrated in Figs. 1-3. It may be pointed out that a

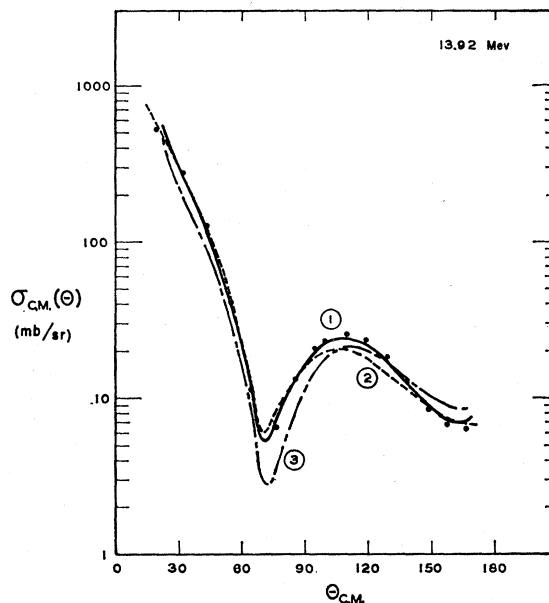


FIG. 1. Comparison of differential elastic scattering cross sections at 13.92 Mev (Tokyo data<sup>3</sup>) associated with various values of  $\chi^2$ . The dots are experimental points. Curve 1 is the optimum fit, for which  $\chi_\sigma^2=50$ . The value of  $\chi_\sigma^2$  is 200 for curve 2 and 1300 for curve 3. All theoretical curves are the results of a search at different grid points.

<sup>13</sup> M. A. Melkanoff, J. S. Nodvik, D. S. Saxon, and D. G. Cantor, *A Fortran Program for Elastic Scattering Analyses with the Nuclear Optical Model* (University of California Press, Berkeley and Los Angeles, California, 1961).

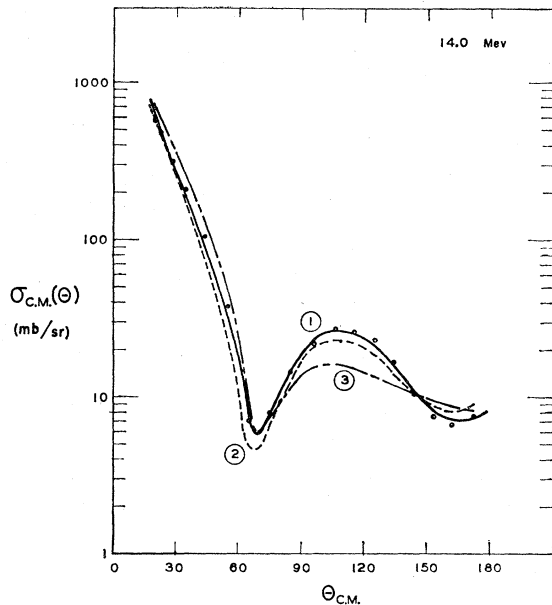


FIG. 2. Comparison of differential elastic scattering cross sections at 14.0 Mev (Princeton data<sup>4,5</sup>) associated with various values of  $\chi_\sigma^2$ . The dots are experimental points. Curve 1 is the optimum fit, for which  $\chi_\sigma^2=400$ . The value of  $\chi_\sigma^2$  is 1600 for curve 2 and 8800 for curve 3. All theoretical curves are the results of a search at different grid points.

deviation of  $\chi_\sigma^2$  by a factor of 2, in the neighborhood of the optimum fit, is hardly discernible. Although such a deviation in  $\chi_P^2$  appears more noticeable, it was not considered significant because of the large experimental errors in the polarization. In judging the quality of the fits to the experimental cross sections, the following approximate scale may be useful:

*Tokyo data*<sup>3</sup>

- $\chi_\sigma^2 \lesssim 300$  good
- $\chi_\sigma^2 \sim 500$  fair
- $\chi_\sigma^2 \gtrsim 900$  unacceptable

*Princeton data*<sup>4-6</sup>

- $\chi_\sigma^2 \lesssim 700$  good
- $\chi_\sigma^2 \sim 1200$  fair
- $\chi_\sigma^2 \gtrsim 2200$  unacceptable.

The preceding scale is, of course, a purely subjective one and is based on a visual evaluation of the quality of the fits.

## V. RESULTS

### A. Low-Energy Analysis ( $7 \text{ Mev} \lesssim E_{\text{lab}} \lesssim 12 \text{ Mev}$ )

Below 11 or 12 Mev, it is often difficult, if not impossible, to obtain reasonable fits to the experimental differential cross sections. The occasional fits which can be obtained often require pathological values for the parameters. There appeared to be two sources of difficulty at the low energies. First, the tendency of

the theoretical differential cross sections to fall below the experimental ones suggests the presence of strong compound elastic scattering in this region. Although this tendency persists at higher energies, it becomes considerably less pronounced above 14 Mev. Furthermore, the optimum fits at the low energies are often characterized by negative values of  $W_1$  and by small or even negative reaction cross sections. A second source of difficulty is the presence of narrow energy bands in which the nature of the cross-section curves changes radically. These anomalous angular distributions cannot adequately be reproduced by the optical model, as illustrated in Fig. 4. If, indeed, such anomalies are associated with compound nucleus resonances, as Nagahara suggests,<sup>3</sup> this failure of the model is not unexpected.

### B. Medium-Energy Analysis ( $12 \text{ Mev} \lesssim E_{\text{lab}} \lesssim 20 \text{ Mev}$ )

Above 11 or 12 Mev it is possible to obtain satisfactory fits to the experimental data. The results obtained by the grid-search procedure described in Sec. IV for the values of the parameters corresponding to the optimum fits, together with the associated values of  $\chi_\sigma^2$ ,  $\chi_P^2$ ,  $\chi^2$ , and the reaction cross section,  $\sigma_R$ , are presented in Table II. The following features of these results may be noted: (1) with a few exceptions, the

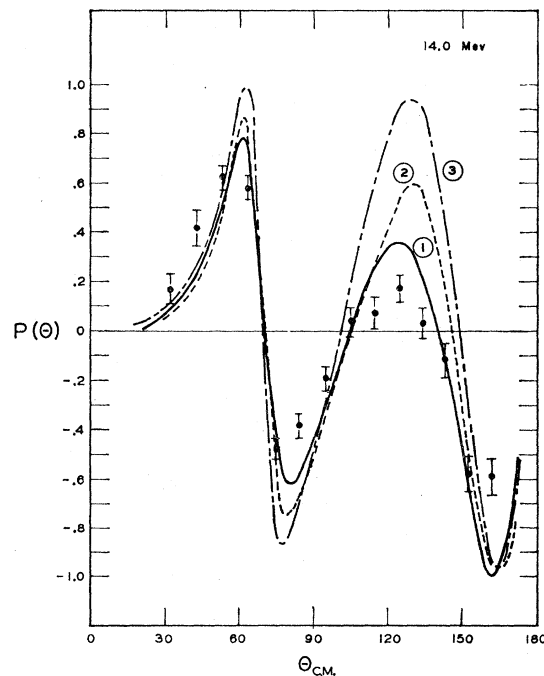


FIG. 3. Comparison of polarizations at 14.0 Mev (Osaka data<sup>8</sup>) associated with various values of  $\chi_P^2$ . The dots are experimental points. The value of  $\chi_P^2$  is 115 for curve 1, 290 for curve 2, and 800 for curve 3. All theoretical curves are the results of a search at different grid points. Curve 2 is the polarization corresponding to the optimum fit, for which  $\chi^2 = \chi_\sigma^2 + \chi_P^2$  is a minimum.

optimum fits occur at  $R_0=1.30$  f for  $E_{lab} \leq 14$  Mev, at  $R_0=1.25$  f for  $14 \text{ Mev} \leq E_{lab} \leq 15.2$  Mev, and at  $R_0=1.20$  f for  $E_{lab} > 15.2$  Mev; (2) all optimum fits below 17.8 Mev are characterized by the same two grid parameter values,  $b=0.25$  f and  $W=0$ ; (3) the optimum fits for  $17.8 \text{ Mev} \leq E_{lab} \leq 18.9$  Mev are characterized by a broadening of the absorptive part of the potential, this broadening occurring in the form of increased  $b$ , increased  $W$ , or both.

In view of the energy dependence of the radius parameter characterizing the optimum fits, it was decided to examine deviations from the optimum fit parameters for the purpose of determining whether satisfactory fits over the entire medium energy range can be obtained with a constant value of  $R_0$ . In this connection, the results of the grid-search analysis show that the radius parameter  $R_0=1.10$  f cannot be used, inasmuch as the best fits obtainable with this value are definitely not acceptable for a large number of energies. For the same reason, the radius parameter  $R_0=1.30$  f must be ruled out, even though satisfactory fits can be obtained below 14 or 15 Mev. Consequently, if the radius parameter is restricted to remain constant over the entire medium energy range, its value cannot be as large as 1.30 f or as small as 1.10 f.

On the other hand, it is possible to obtain satisfactory agreement with the experimental cross-section and polarization data throughout the medium energy range

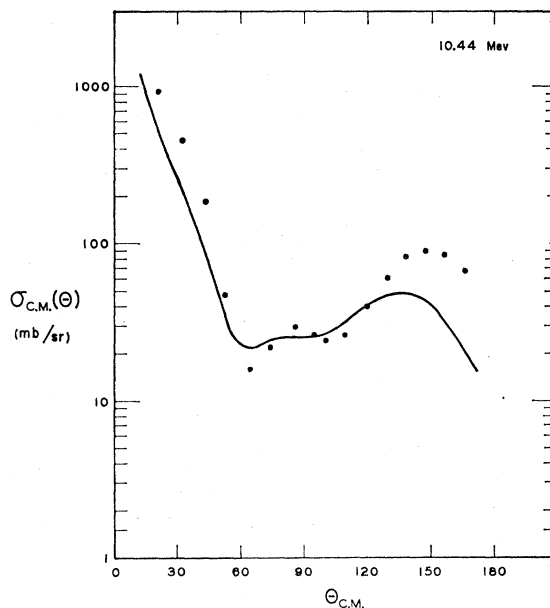


FIG. 4. Comparison of theoretical and experimental differential elastic scattering cross sections at 10.44 Mev, illustrating the difficulties encountered at low energies. The dots are experimental points.<sup>3</sup> The theoretical curve corresponds to the optimum fit, for which  $\chi^2$  is a minimum. The parameters are:  $R_0=1.30$  f,  $b=0.75$  f,  $V=50$  Mev,  $W=4$  Mev,  $W_1=0.08$  Mev,  $a=0.57$  f,  $V_S=-9.7$  Mev,  $W_S=0$ .

TABLE II. Optical-model parameters corresponding to optimum fits.

$E_{lab}$ (Mev)	Data references	$R_0$ (fermi)	$b$ (fermi)	$V$ (Mev)	$W$ (Mev)	$W_1$ (Mev)	$a$ (fermi)	$V_S$ (Mev)	$\chi^2$	$\chi P^2$	$\chi^2$	$\sigma_R$ (mb)
11.85	2, 7	1.30	0.25	52.0	0	20.1	0.45	-5.1	165	277	442	368
12.07	3, 7	1.30	0.25	53.0	0	17.6	0.33	-6.6	515	385	900	335
12.25	3, 7	1.25	0.25	58.1	0	15.7	0.30	-6.3	397	418	815	281
12.43	3, 7	1.30	0.25	51.9	0	19.4	0.35	-6.0	368	365	733	344
12.67	3, 7	1.30	0.25	51.5	0	19.2	0.34	-6.0	307	404	711	339
13.06 <sup>a</sup>	3, 8	1.30	0.25	51.1	0	19.9	0.42	-4.0	378	321	699	346
13.21 <sup>a</sup>	3, 8	1.30	0.25	50.6	0	27.4	0.41	-3.6	538	300	838	381
13.35	3, 8	1.30	0.25	48.6	0	27.1	0.40	-5.7	579	484	1063	393
13.48	3, 8	1.25	0.25	52.1	0	26.9	0.42	-6.6	318	363	681	382
13.64	3, 8	1.20	0.25	56.8	0	23.3	0.40	-5.9	116	228	344	336
13.92	3, 8	1.20	0.25	55.4	0	21.7	0.44	-5.6	49	195	244	340
14.0	4, 5, 8	1.20	0.25	58.2	0	19.9	0.40	-6.0	401	291	692	317
14.36	3, 8	1.25	0.25	52.6	0	19.0	0.46	-5.7	172	299	471	352
14.7	4, 5, 8	1.25	0.25	53.0	0	21.2	0.4,	-6.4	239	331	570	374
14.94	3, 8	1.25	0.25	52.9	0	21.1	0.45	-6.4	264	347	611	372
15.11	3, 8	1.20	0.25	58.7	0	17.0	0.40	-6.1	106	280	386	302
15.2	4, 5, 8	1.25	0.25	53.4	0	17.9	0.38	-6.3	773	385	1158	332
15.37	3, 8	1.20	0.25	57.6	0	16.8	0.41	-5.8	120	264	384	298
15.50	3, 8	1.20	0.25	57.2	0	16.7	0.42	-5.5	74	246	320	295
15.6	4, 5, 8	1.20	0.25	56.9	0	17.1	0.40	-5.9	1286	269	1555	301
15.66	3, 8	1.20	0.25	57.1	0	17.1	0.41	-5.6	55	264	319	297
15.79	3, 8	1.20	0.25	56.9	0	17.7	0.42	-5.4	42	258	300	303
15.92	3, 8	1.20	0.25	56.8	0	16.7	0.41	-5.4	30	262	292	292
16.2	4, 5, 8	1.20	0.25	55.1	0	17.5	0.43	-5.3	912	249	1161	303
16.7	4, 5, 8	1.20	0.25	56.1	0	19.1	0.44	-5.2	282	285	567	317
17.4	4, 5, 9	1.20	0.25	55.9	0	17.7	0.39	-5.5	367	586	953	297
17.8	4, 5, 9	1.20	0.75	51.4	2	5.6	0.50	-4.1	246	565	811	387
18.4	6, 9	1.20	0.6	54.4	0	9.9	0.51	-2.7	75	615	690	378
18.9	4, 5, 9	1.20	0.25	53.7	2	18.3	0.54	-2.7	732	697	1429	376
19.4	4, 9	1.25	0.25	51.0	0	23.2	0.49	-4.8	868	681	1549	372

<sup>a</sup> At 13.06 and 13.21 Mev the optimum fits actually occurred at  $R_0=1.10$  f but these were rejected because of the anomalously low reaction cross sections ( $\sigma_R < 10$  mb) which resulted.

TABLE III. Compromise parameters for  $R_0=1.20$  f. Best possible fits obtainable with  $R_0=1.20$  f are designated by an asterisk. The latter part of the table presents an alternate set of parameters for the higher energies.

$E_{lab}$ (Mev)	$b$ (fermi)	$V$ (Mev)	$W$ (Mev)	$W_1$ (Mev)	$a$ (fermi)	$V_S$ (Mev)	$\chi_\sigma^2$	$\chi_P^2$	$\chi^2$	$\sigma_R$ (mb)
11.85	0.25	61.5	0	11.6	0.34	-4.8	427	503	930	226
12.07	0.25	63.8	0	10.2	0.24	-6.4	546	648	1194*	201
12.25	0.25	63.5	0	10.7	0.25	-6.1	365	607	972*	203
12.43	0.25	62.9	0	11.1	0.25	-5.9	355	591	946*	203
12.67	0.25	62.7	0	12.9	0.26	-5.9	345	533	878*	222
13.06	0.25	61.2	0	11.5	0.31	-4.2	506	633	1139	196
13.21	0.25	62.7	0	15.9	0.26	-4.3	308	753	1061	211
13.35	0.25	60.9	0	23.2	0.28	-5.8	624	804	1428*	286
13.48	0.25	59.6	0	21.1	0.29	-6.4	532	702	1234	294
13.64	0.25	56.8	0	23.3	0.40	-5.9	116	228	344*	336
13.92	0.25	55.4	0	21.7	0.44	-5.6	49	195	244*	340
14.0	0.25	58.2	0	19.9	0.40	-6.0	401	291	692*	317
14.36	0.25	56.5	0	18.9	0.46	-5.7	301	224	525*	327
14.7	0.25	57.1	0	21.7	0.46	-6.5	422	249	671*	353
14.94	0.25	57.2	0	21.0	0.44	-6.5	405	275	680*	344
15.11	0.25	58.7	0	17.0	0.40	-6.1	106	280	386*	302
15.2	0.25	58.2	0	17.9	0.40	-6.3	941	301	1242*	310
15.37	0.25	57.6	0	16.8	0.41	-5.8	120	264	384*	298
15.50	0.25	57.2	0	16.7	0.42	-5.5	74	246	320*	295
15.6	0.25	56.9	0	17.1	0.40	-5.9	1286	269	1555*	301
15.66	0.25	57.1	0	17.1	0.41	-5.6	55	264	319*	297
15.79	0.25	56.8	0	17.7	0.42	-5.4	42	258	300*	303
15.92	0.25	56.8	0	16.7	0.41	-5.4	30	262	292*	292
16.2	0.25	55.1	0	17.5	0.43	-5.3	912	249	1161*	303
16.7	0.25	56.1	0	19.1	0.44	-5.2	282	285	567*	317
17.4	0.25	55.9	0	17.7	0.39	-5.5	367	586	953*	297
17.8	0.25	51.5	4	12.4	0.52	-3.8	698	684	1382	379
18.4	0.25	54.2	2	17.9	0.51	-2.6	539	654	1193	363
18.9	0.25	53.7	2	18.3	0.54	-2.7	732	697	1429*	376
19.4	0.25	53.3	2	20.7	0.53	-5.1	1317	787	2104	392
17.8	0.50	51.7	4	6.5	0.52	-4.0	292	656	948	397
18.4	0.50	55.0	0	11.5	0.50	-2.7	210	617	827	361
18.9	0.50	53.1	0	11.2	0.53	-2.8	876	638	1514	361
19.4	0.50	53.5	0	12.4	0.52	-5.0	1032	677	1709*	382

with the radius parameter  $R_0=1.20$  f. In discussing the results for this case, presented in Table III, it is convenient to divide the energy range under consideration into three intervals. For  $13.64 \text{ Mev} \leq E_{lab} \leq 17.4 \text{ Mev}$ , the results presented in Table III correspond to the best fits obtainable with  $R_0=1.20$  f. Without exception, these are characterized by the grid parameter values  $b=0.25$  f and  $W=0$ . Furthermore, as may be seen by comparing Tables II and III, most of these best fits are also optimum fits. The over-all agreement between theoretical and experimental cross sections over this energy interval is quite good.

For  $11.85 \text{ Mev} \leq E_{lab} < 13.64 \text{ Mev}$ , the best fits obtainable with  $R_0=1.20$  f are characterized by the values  $b=0.25$  f and  $W=0$  for approximately half of the energies investigated, and it is possible to obtain acceptable fits with these same values throughout this lower energy interval. The results presented in Table III for  $11.85 \text{ Mev} \leq E_{lab} < 13.64 \text{ Mev}$  correspond, in any case, to the best fits obtainable with  $R_0=1.20$  f and  $b=0.25$  f. Although the quality of the corresponding fits to the polarization data is somewhat inferior to that obtained with the optimum fits (Table II), the quality of the fits to the differential cross sections is not markedly different.

The higher energy interval,  $17.8 \text{ Mev} \leq E_{lab} \leq 19.4 \text{ Mev}$ , is characterized by a broadening of the absorptive shell, as evidenced by the fact that no acceptable fits can be obtained at  $17.8 \text{ Mev}$  with  $b=0.25$  f and  $W=0$ . Because of the strong coupling between the parameters  $b$  and  $W$  in this region, these parameters cannot be determined separately with any precision. Two sets of parameters are presented in Table III for  $E_{lab} \geq 17.8 \text{ Mev}$ ; the first set corresponds to the best fits obtainable with  $R_0=1.20$  f and  $b=0.25$  f, and the second set corresponds to the best fits with  $R_0=1.20$  f and  $b=0.50$  f. As may be seen from Table III, although the values of  $W_1$  are larger for the first set, there is very little difference between corresponding values of  $V$ ,  $V_S$ ,  $a$ , and  $\sigma_R$  for the two sets. Furthermore, both sets of parameters yield acceptable fits to the experimental data, although the agreement obtained with the second set is somewhat better.

In contrast to the satisfactory over-all agreement between experimental and theoretical differential cross sections and polarizations obtainable with the radius parameter  $R_0=1.20$  f, serious difficulties arise in connection with the reaction cross section. As will be discussed in Sec. VI, the values of  $\sigma_R$  given in Table III are generally too low and are even smaller than the

TABLE IV. Compromise parameters for  $R_0=1.25$  f. All results correspond to best possible fits obtainable with  $R_0=1.25$  f except those for 11.85 and 18.4 Mev.

$E_{lab}$ (Mev)	$b$ (fermi)	$V$ (Mev)	$W$ (Mev)	$W_1$ (Mev)	$a$ (fermi)	$V_S$ (Mev)	$\chi_\sigma^2$	$\chi_P^2$	$\chi^2$	$\sigma_R$ (mb)
11.85	0.25	56.8	0	16.7	0.39	-5.4	364	293	657	302
12.07	0.25	58.6	0	13.7	0.27	-6.6	505	489	994	263
12.25	0.25	58.1	0	15.7	0.30	-6.3	397	418	815	281
12.43	0.25	57.4	0	15.7	0.30	-6.0	376	450	826	274
12.67	0.25	56.9	0	17.2	0.31	-6.0	355	418	773	291
13.06	0.25	54.8	0	20.1	0.42	-3.7	703	237	940	322
13.21	0.25	57.3	0	19.5	0.27	-4.2	314	764	1078	260
13.35	0.25	53.7	0	28.2	0.38	-6.0	668	436	1104	365
13.48	0.25	52.1	0	26.9	0.42	-6.6	318	363	681	382
13.64	0.25	52.1	0	24.2	0.42	-5.8	187	292	479	368
13.92	0.25	51.2	0	21.0	0.43	-5.5	84	277	361	355
14.0	0.25	51.8	0	18.4	0.39	-5.7	703	353	1056	328
14.36	0.25	52.6	0	19.0	0.46	-5.7	172	299	471	352
14.7	0.25	53.0	0	21.2	0.45	-6.4	239	331	570	374
14.94	0.25	52.9	0	21.1	0.45	-6.4	264	347	611	372
15.11	0.25	54.2	0	16.9	0.38	-6.1	56	365	421	323
15.2	0.25	53.4	0	17.9	0.38	-6.3	773	385	1158	332
15.37	0.25	53.1	0	17.4	0.40	-5.9	109	327	436	329
15.50	0.25	52.9	0	16.7	0.40	-5.6	80	320	400	316
15.6	0.25	52.3	0	17.1	0.39	-5.9	1468	341	1809	321
15.66	0.25	52.7	0	17.9	0.41	-5.5	107	320	427	330
15.79	0.25	52.5	0	17.9	0.41	-5.5	104	325	429	327
15.92	0.25	52.4	0	17.4	0.41	-5.4	78	319	397	323
16.2	0.25	51.0	0	17.3	0.40	-5.4	1224	317	1541	320
16.7	0.25	51.9	0	18.8	0.41	-5.4	918	347	1265	333
17.4	0.25	51.2	0	17.7	0.37	-5.5	1651	677	2328	317
17.8	0.25	49.0	4	12.1	0.50	-3.9	181	774	955	402
18.4	0.25	51.0	2	17.9	0.50	-2.7	105	701	806	391
18.9	0.25	50.2	0	20.6	0.49	-2.8	789	660	1449	347
19.4	0.25	51.0	0	23.2	0.49	-4.8	868	681	1549	372

$(p, p')$  cross section to the 4.4-Mev state of  $C^{12}$  for  $E_{lab} < 13.2$  Mev. This difficulty prompted a consideration of the larger radius parameter  $R_0=1.25$  f.

With two exceptions, the results presented in Table IV correspond to the best possible fits obtainable with  $R_0=1.25$  f. (For  $E_{lab}=11.85$  and 18.4 Mev, the results for the best fits obtainable with  $R_0=1.25$  f,  $b=0.25$  f are given.) As may be seen by comparing Tables III and IV, the quality of the corresponding fits to the differential cross sections and polarizations obtainable with the radius parameters  $R_0=1.20$  f and  $R_0=1.25$  f is not significantly different except at  $E_{lab}=16.7$  and 17.4 Mev, where the quality of the fits obtained with  $R_0=1.25$  f is noticeably inferior. The main feature of the results for the two values of the radius parameter is the same: the absorption is confined to a thin shell characterized by  $b=0.25$  f,  $W=0$  for energies below  $E_{lab}=17.8$  Mev, at which energy the region of absorption suddenly broadens. With the radius parameter  $R_0=1.25$  f, a broadening in the form of increased  $W$ , confined to the interval  $17.4 \text{ Mev} < E_{lab} < 18.9$  Mev, seems to be preferred. However, because of the strong coupling between the parameters  $b$  and  $W$ , a broadening in the form of increased  $b$  cannot be ruled out. Furthermore, for  $E_{lab} \geq 18.9$  Mev, acceptable fits may also be obtained with slightly increased values of  $b$  or  $W$ , e.g., with  $b=0.25$  f,  $W=2$  Mev, or with  $b=0.40$  f,  $W=0$ .

A comparison of theoretical and experimental differ-

ential elastic cross sections and polarizations at various energies is shown in Figs. 5-9.

## VI. DISCUSSION

### A. Energy Dependence of Parameters

As noted in the previous section, the most striking features of the results of the analysis are the narrowness of the region over which the absorption takes place for energies below  $E_{lab}=17.8$  Mev, and the sudden broadening of the absorption region at this energy. These aspects of the results are illustrated in Fig. 10, in which the absorptive part of the central nuclear potential,  $\text{Im}(V_{CN})$ , corresponding to the parameters given in Table III for  $R_0=1.20$  f, is shown as a function of  $r$  and  $E_{lab}$ .

The abrupt change in absorption between 17.4 and 17.8 Mev is difficult to understand. Reactions whose thresholds occur below 17 Mev include  $(p, \alpha)$ ,  $(p, p')$ , and  $(p, 3\alpha)$ . The  $(p, \alpha)$  reaction has been investigated<sup>14</sup> and cannot account for the anomaly. The  $(p, p')$  reactions involving the first three excited states of  $C^{12}$  show no marked structure as a function of energy in this region.<sup>4</sup> Little is known about the  $(p, p')$  cross sections to higher excited states or about the  $(p, 3\alpha)$  reaction. Reactions whose thresholds lie in the neighborhood of the anomaly include the  $(p, d)$ ,  $(p, 2p)$ , and

<sup>14</sup> J. B. Reynolds, Phys. Rev. 98, 1289 (1955).

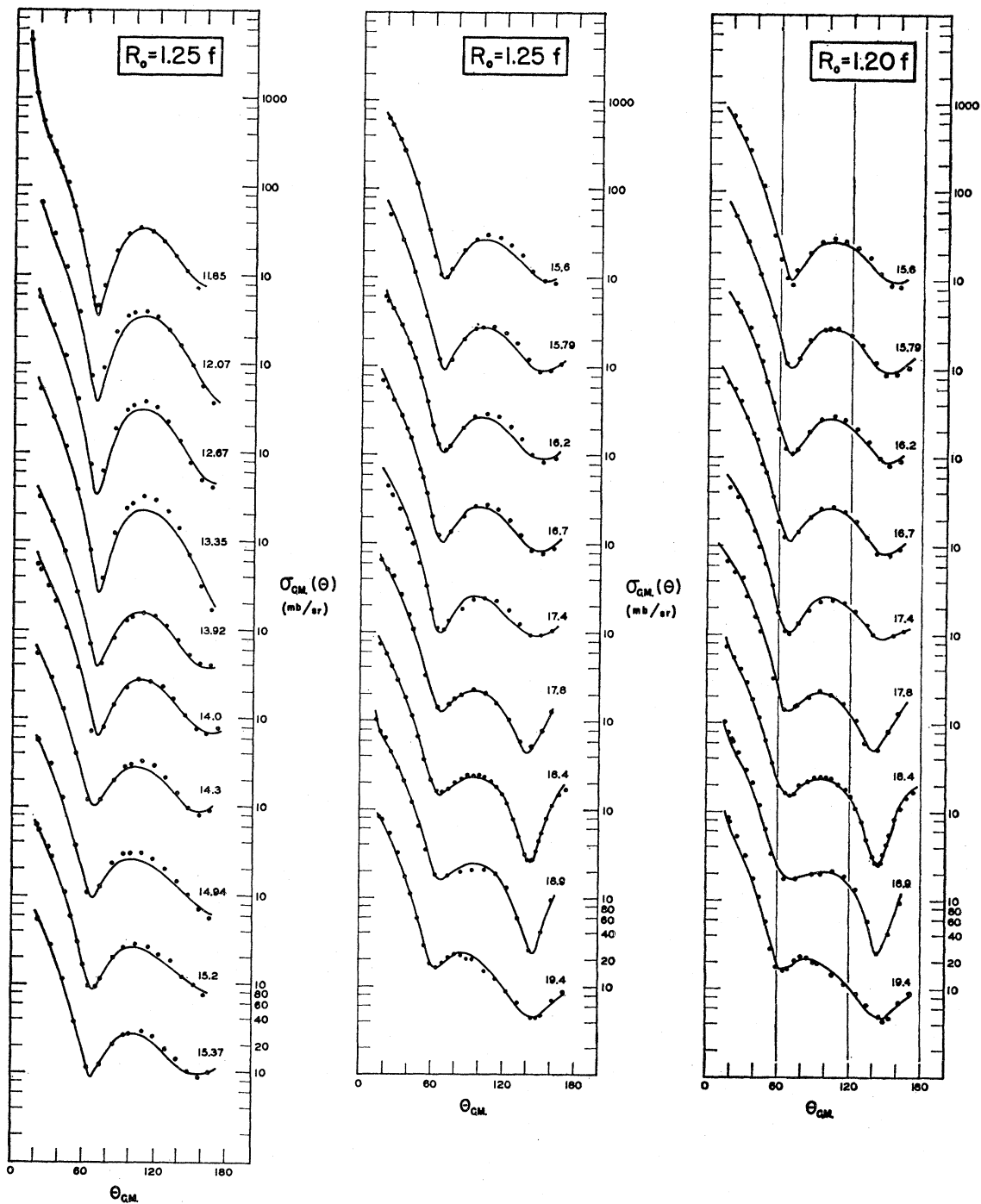


FIG. 5. Comparison of theoretical and experimental differential elastic scattering cross sections at various energies. The dots are experimental points. In nearly all cases, the theoretical curves labelled  $R_0=1.25$  f correspond to the best fits obtainable with  $R_0=1.25$  f and the curves labelled  $R_0=1.20$  f correspond to the optimum fits; the associated parameters are listed in Tables II and IV. The exceptions are as follows: At 11.85 and 18.4 Mev, the curves labelled  $R_0=1.25$  f correspond to the best fits obtainable with  $R_0=1.25$  f and  $b=0.25$  f; the associated parameters are listed in Table IV. At 19.4 Mev, the curve labelled  $R_0=1.20$  f is not the optimum fit but is the best obtainable with  $R_0=1.20$  f; the associated parameters are given in the last entry of Table III.

several  $(p,p')$  channels. Since the threshold for the  $(p,d)$  reaction lies at  $E_{\text{lab}}=17.9$  Mev, this reaction could affect the 17.8-Mev data only through imperfect energy

resolution. No information is available on the  $(p,2p)$  reaction or on the energy dependence of the cross sections for the  $(p,p')$  channels which open up in this

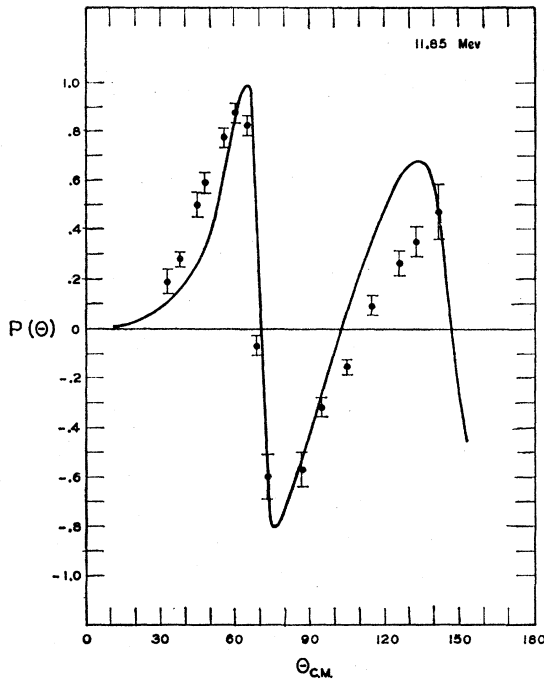


FIG. 6. Comparison of experimental and theoretical polarizations at 11.85 Mev. The dots are experimental points. The parameters corresponding to the theoretical curve are given in Table IV.

region. However, if the cross section for the  $(p,2p)$  reaction rises rapidly above threshold, as is the case for the  $(p,pn)$  reaction, then the  $(p,2p)$  reaction could be a primary factor in accounting for the anomaly.

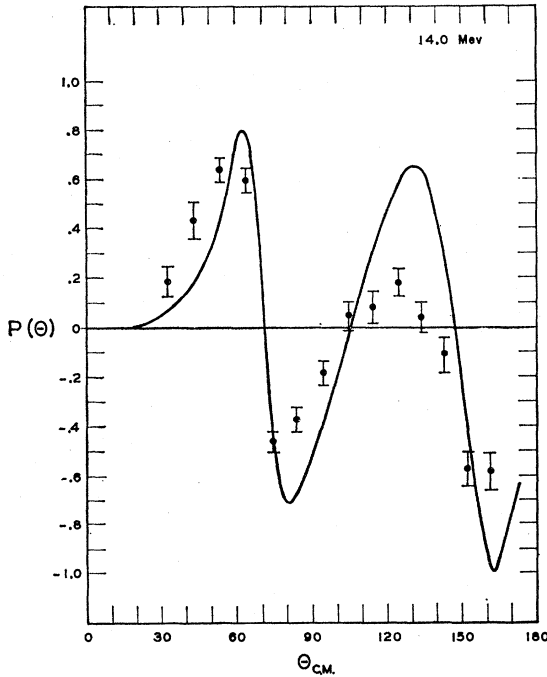


FIG. 7. Comparison of experimental and theoretical polarizations at 14.0 Mev. The dots are experimental points. The parameters corresponding to the theoretical curve are given in Table IV.

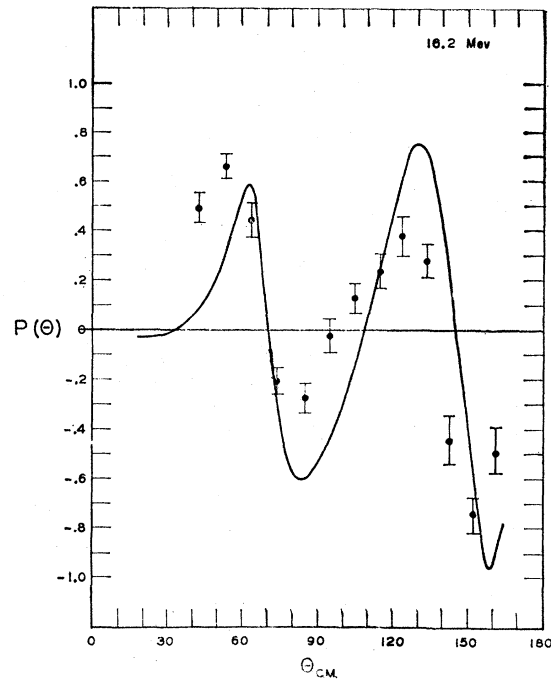


FIG. 8. Comparison of experimental and theoretical polarizations at  $E_{lab}=16.2$  Mev. The dots are experimental points for  $E_{lab}=16.0$  Mev. The parameters corresponding to the theoretical curve are given in Table IV.

On the whole, the values of the parameters  $V$ ,  $W_1$ ,  $V_s$ , and  $a$  listed in Tables II-IV are in accord with values previously quoted for similar analyses.<sup>1</sup> The

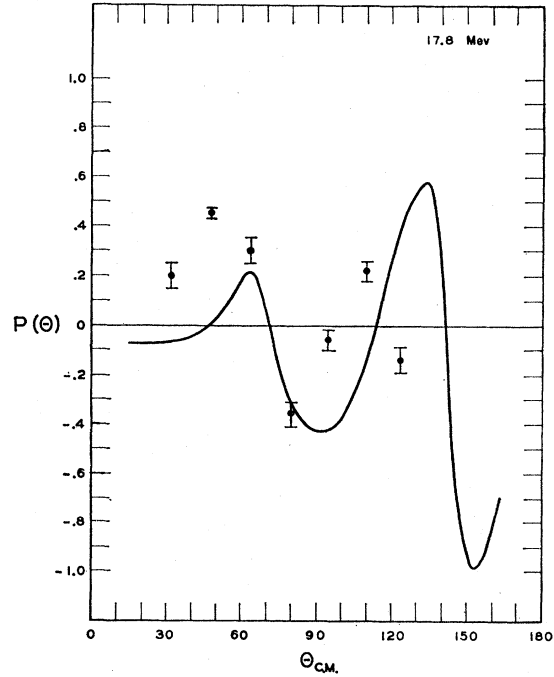


FIG. 9. Comparison of experimental and theoretical polarizations at 17.8 Mev. The dots are experimental points. The parameters corresponding to the theoretical curve are given in Table IV.

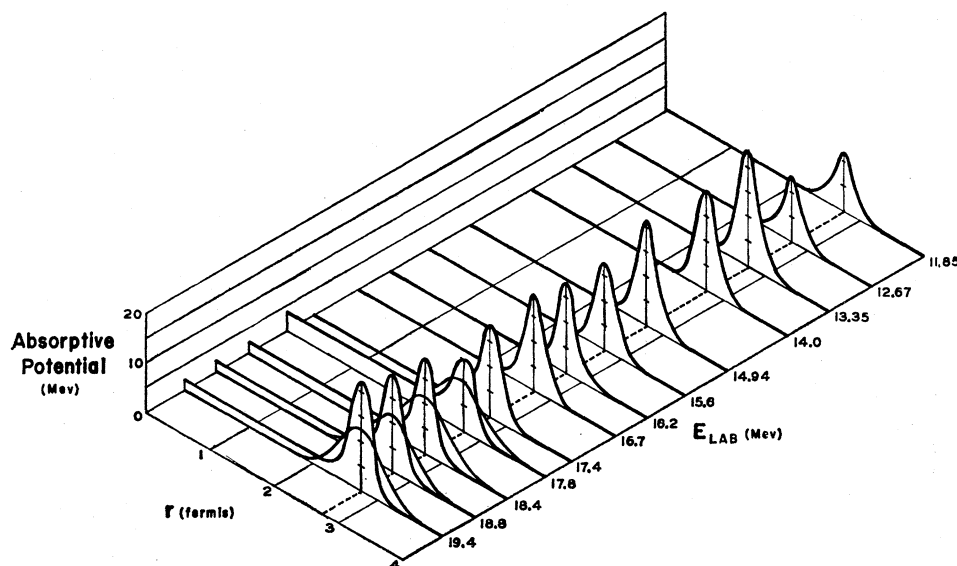


FIG. 10. Absorptive part of the optical-model potential as a function of  $r$  and  $E_{\text{lab}}$  for  $R_0=1.20$  f. Below 17.8 Mev the curves correspond to the best fits obtainable with  $R_0=1.20$  f and  $b=0.25$  f. The two sets of curves at the higher energies correspond to the best fits obtainable with  $R_0=1.20$  f,  $b=0.25$  f, and  $R_0=1.20$  f,  $b=0.50$  f. The associated parameters are given in Table III.

behavior of these parameters as a function of energy for the radius parameter  $R_0=1.25$  f (Table IV) is shown in Fig. 11. The corresponding behavior for the radius parameter  $R_0=1.20$  f is not illustrated but is quite similar to that for  $R_0=1.25$  f. As may be seen from Fig. 11, the depth of the real part of the central potential exhibits a slight dip near  $E_{\text{lab}}=14$  Mev but otherwise decreases slowly and monotonically with

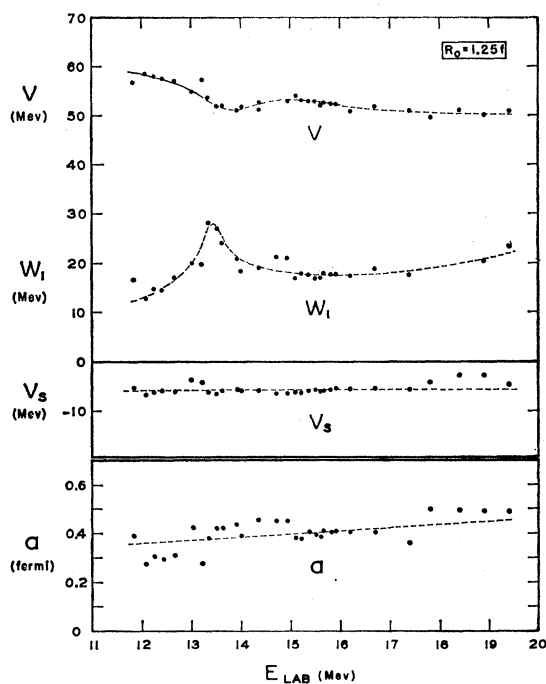


FIG. 11. Energy dependence of the parameters  $V$ ,  $W_1$ ,  $V_s$ , and  $a$  for  $R_0=1.25$  f. The values plotted are listed in Table IV. At 17.8 and 18.4 Mev, the values of  $W_1$  have been omitted since the parameter  $W$  is different from zero at these energies.

energy. The surface absorption parameter,  $W_1$ , rises rather sharply between 12 and 13 Mev, peaks near  $E_{\text{lab}}=13.2$  Mev, and then remains more or less constant for energies above 14 Mev. There appears to be a correlation between the dip in  $V$  and the peaking in  $W_1$ , which may, however, be coincidental. The real part of the spin-orbit strength,  $V_s$ , remains constant at approximately  $-5$  Mev, except for a dip at the higher energies. Although the behavior of the rounding parameter,  $a$ , is somewhat obscured by the large scatter, there is a definite tendency for this parameter to increase with energy. The small values of  $a$  which occur between 12 and 13 Mev may be due in part to the presence of compound elastic scattering. The latter would have the effect of increasing the scattering at larger angles, and this increase may be simulated, to a certain extent, by the increase in reflection obtained with smaller values of  $a$ .

## B. Reaction Cross Sections

The theoretically predicted reaction cross sections are compared with the available experimental data in Figs. 12 and 13. The theoretical values corresponding to the radius parameter  $R_0=1.20$  f (Table III) are plotted in Fig. 12, those corresponding to  $R_0=1.25$  f (Table IV) in Fig. 13. The experimental data shown include preliminary measurements of  $\sigma_R$  at various energies<sup>15</sup> and the measured  $(p,p')$  cross section to the 4.4-Mev state of  $C^{12}$ .<sup>3</sup>

As may be seen from Fig. 12, the theoretical reaction cross sections obtained with the radius parameter  $R_0=1.20$  f generally fall below the experimental ones. This discrepancy is particularly serious for energies below 13.2 Mev, where the theoretical values are even

<sup>15</sup> R. Pollock (private communication).

less than the partial cross section to the first excited state. With the larger radius parameter,  $R_0=1.25$  f, the agreement between theoretical and experimental values is considerably improved, especially at the lower energies. However, as may be seen from Fig. 13, the theoretical values still exhibit a tendency to be somewhat low.

It should be remarked that the large drop in the theoretical reaction cross section for energies below 13.2 Mev does not occur with the optimum fits, which are characterized by the radius parameter  $R_0=1.30$  f at the lower energies. Accurate measurements of the reaction cross section, therefore, may prove to be a test of the necessity to constrain  $R_0$  to a fixed value over a range of energies.

### C. Polarizations

As previously mentioned, the polarization data which lay closest in energy to each set of differential cross sections were analyzed together with this set. Although such an extrapolation might be questioned, it did not appear to have a serious effect upon the final results. The relatively large uncertainties in the experimental polarization data relegating them to a secondary role in the analysis, the minimum value of  $\chi^2$  representing a compromise between  $\chi_{\sigma}^2$  and  $\chi_P^2$  in which  $\chi_{\sigma}^2$  is usually the most significant factor. In addition, several analyses limited to the differential cross sections yielded results quite similar to those obtained when the polarization data were included. In retrospect, the primary function of the polarization data seems to have been that of determining the sign of  $V_s$ . If more accurate measurements were available it is likely that the polarization would assume a more significant role in the determination of the parameters.

### D. Definiteness of the Parameters

The determination of the precise limits on the domain of acceptability of the parameters is complicated by

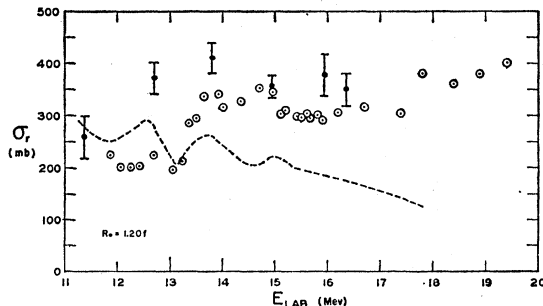


FIG. 12. Comparison of theoretical reaction cross sections with experimental results. The circles correspond to theoretical reaction cross sections obtained with  $R_0=1.20$  f and  $b=0.25$  f; the associated parameters are given in Table III. The flags correspond to preliminary measurements<sup>15</sup> of the reaction cross section. The dashed curve is the measured cross section for inelastic scattering to the 4.4-Mev state of carbon.<sup>3</sup>

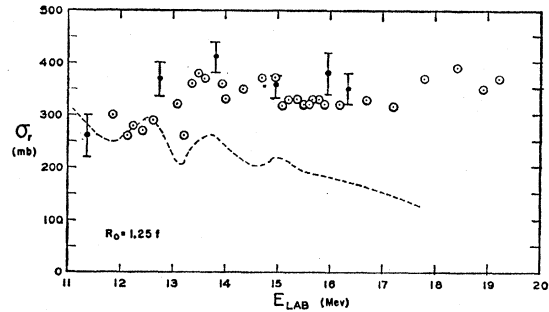


FIG. 13. Comparison of theoretical reaction cross sections with experimental results. The circles correspond to theoretical reaction cross sections obtained with  $R_0=1.25$  f; the associated parameters are given in Table IV. The flags correspond to preliminary measurements<sup>15</sup> of the reaction cross section. The dashed curve is the measured cross section for inelastic scattering to the 4.4-Mev state of carbon.<sup>3</sup>

the high dimensionality of the parameter space. During the course of the analysis, however, some information was obtained concerning the extent to which the parameters which yield acceptable fits are unique. In particular, the following statements can be made about the grid parameters. If the radius parameter  $R_0$  is restricted to remain constant over the entire medium-energy range,  $11.85 \text{ Mev} \leq E_{\text{lab}} \leq 19.4 \text{ Mev}$ , this parameter cannot be as small as 1.1 f or as large as 1.3 f. If the quantities  $b$  and  $W$  are similarly restricted over the range,  $11.85 \text{ Mev} \leq E_{\text{lab}} \leq 17.4 \text{ Mev}$ , then  $b$  must be less than 0.50 f and  $W$  less than 2 Mev.

The coupling between the absorption parameters  $b$  and  $W$  for a typical energy ( $E_{\text{lab}}=14$  Mev) is illustrated in Fig. 14, which shows the contours of equal  $\chi^2$  in the  $b$ - $W$  plane with  $R_0=1.20$  f and with the values of the parameters  $V$ ,  $W_1$ ,  $V_s$ , and  $a$  chosen so as to minimize  $\chi^2$  for given  $b$ ,  $W$ , and  $R_0$ . The contours of constant reaction cross section, obtained under the same con-

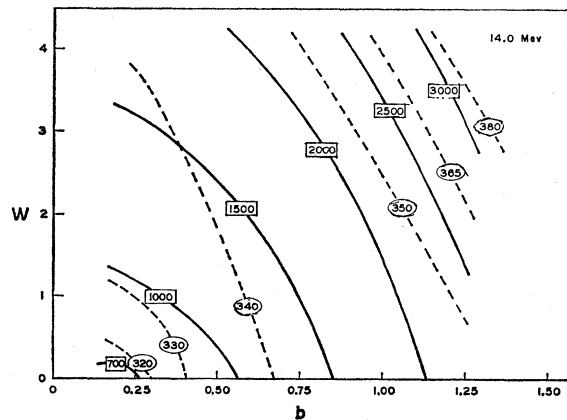


FIG. 14. Contours of constant  $\chi^2$  and reaction cross section in the  $b$ - $W$  plane for  $R_0=1.20$  f at 14.0 Mev. The solid curves are contours of constant  $\chi^2$  in the neighborhood of the optimum fit. The values of other parameters are chosen so as to minimize  $\chi^2$  for given  $b$ ,  $W$ , and  $R_0$ . The dashed curves are contours of constant  $\sigma_r$ (mb) obtained under the same conditions.

TABLE V. Percentage deviations obtained with experimental differential cross sections incremented by +10%. At each energy, the best fit to the renormalized cross-section data and original polarization data was obtained with  $R_0$ ,  $b$ , and  $W$  fixed at the values corresponding to the optimum fit to the original data, given in Table II. The percentage deviation between the values of  $V$ ,  $W_1$ ,  $a$ ,  $V_S$ , and  $\sigma_R$  obtained under these conditions and the corresponding values associated with the optimum fits to the original data are presented.

$E_{lab}$ (Mev)	Percentage deviation from Table II value					$\chi^2$	$\chi^2$ Table II value
	$V$	$W_1$	$a$	$V_S$	$\sigma_R$		
12.25	+0.2	-16.0	-7.2	-2.0	-7.9	520	397
12.67	-1.0	-0.8	+6.2	-0.8	+2.3	632	307
14.0	+1.4	-10.0	-3.5	-2.7	-4.7	836	401
15.66	-1.1	-5.8	+2.7	+0.2	-2.0	190	55
16.2	-1.4	-7.5	+2.3	-0.2	-2.6	2643	912
16.7	-1.8	-8.4	+1.6	-0.8	-3.5	1071	282
17.8	-1.6	-12.5	+2.2	+1.9	-4.7	595	246
18.9	-0.2	-8.8	+3.4	+7.9	-2.4	2512	732

ditions, are also shown. The absolute minimum of  $\chi^2$  lies close to the point  $b=0.25$  f and  $W=0$ , with  $\chi^2$  somewhat less than 700. In this case, the quality of the fits is marginal for values of  $\chi^2$  of the order of 1500. From Fig. 14, it would appear that a sizeable increase in the reaction cross section can be obtained only by deviating significantly from the optimum fit parameters. It should be noted, however, that the values of  $\chi^2$  and  $\sigma_R$  plotted in Fig. 14 correspond to a special cut in the  $\chi^2$  surface. No detailed investigation was made of the behavior for values of  $V$ ,  $W_1$ ,  $V_S$ , and  $a$  which do not minimize  $\chi^2$  for given  $b$ ,  $W$ , and  $R_0$ .

The imaginary part of the spin-orbit coupling strength,  $W_S$ , was put equal to zero throughout most of the analysis. Several preliminary grid searches in which  $W_S$  was permitted to vary, indicated that it almost invariably hovered about zero except in the low-energy region. In this region  $W_S$  often assumed inordinately large values which led to negative reaction cross sections. In general, a value of  $W_S$  of the order of

TABLE VI. Percentage deviations obtained with experimental differential cross sections incremented by -10%. At each energy, the best fit to the renormalized cross-section data and original polarization data was obtained with  $R_0$ ,  $b$ , and  $W$  fixed at the values corresponding to the optimum fit to the original data, given in Table II. The percentage deviation between the values of  $V$ ,  $W_1$ ,  $a$ ,  $V_S$ , and  $\sigma_R$  obtained under these conditions and the corresponding values associated with the optimum fits to the original data are presented.

$E_{lab}$ (Mev)	Percentage deviation from Table II value					$\chi^2$	$\chi^2$ Table II value
	$V$	$W_1$	$a$	$V_S$	$\sigma_R$		
12.25	+0.2	+14.5	+4.3	+1.9	+5.3	270	397
12.67	-0.2	+16.1	+11.5	+1.8	+8.0	193	307
14.0	-1.7	+16.0	+8.0	+3.9	+8.5	338	401
15.66	+0.9	+13.4	+3.7	+1.8	+6.7	28	55
16.2	+1.6	+10.8	-0.5	+0.2	+4.6	206	912
16.7	+1.8	+10.5	-1.4	+1.1	+3.5	187	282
17.8	+2.3	+14.2	-2.6	-3.1	+4.9	364	246
18.9	+1.1	+5.5	-2.5	+8.6	+0.3	233	732

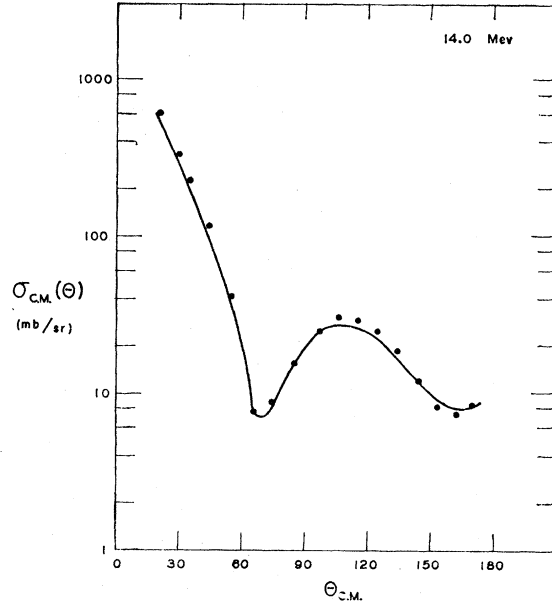


FIG. 15. Optimum fit to the 14-Mev cross-section data incremented by +10%. The parameters corresponding to the theoretical curve are:  $R_0=1.20$  f,  $b=0.25$  f,  $V=59.0$  Mev,  $W=0$ ,  $W_1=17.9$  Mev,  $a=0.39$  f,  $V_S=-6.1$  Mev,  $W_S=0$ .

1 Mev does not appreciably affect the fits and hence cannot be ruled out.

The range of the parameters  $V$ ,  $W_1$ ,  $V_S$ , and  $a$  was not systematically explored since these were not used as grid parameters. Therefore, it is not possible to specify absolute limits on the values of these parameters within which acceptable fits can be obtained. However, relative uncertainties may still be estimated on the basis of experience gained during the course of the analysis:  $\Delta V \sim 2$  Mev,  $\Delta W_1 \sim 1$  to 2 Mev,  $\Delta V_S \sim 1$  to 2 Mev,  $\Delta a \sim 0.05$  Fermi. These quantities should be interpreted as order of magnitude estimates of the changes to be expected in three of the parameters when the fourth is changed by the amount specified.

Additional uncertainties in the values of the parameters may arise from difficulties associated with the normalization of the experimental differential cross sections. In order to estimate the sensitivity of the values of the parameters to changes in normalization, the data at several energies were arbitrarily incremented by  $\pm 10\%$  and subjected to the same grid search procedure as the original data. The results are summarized in Tables V and VI. These tables were constructed by comparing, at that grid point corresponding to the optimum fit to the original data, the values of the parameters  $V$ ,  $W_1$ ,  $V_S$ , and  $a$ , obtained before and after the 10% renormalization. The tables show that except for  $W_1$  the values of the parameters are relatively insensitive to changes in normalization. In fact, the changes in  $V$ ,  $V_S$ , and  $a$  resulting from the renormalization procedure are less than the scatter in the values of the parameters which are plotted in Fig. 11.

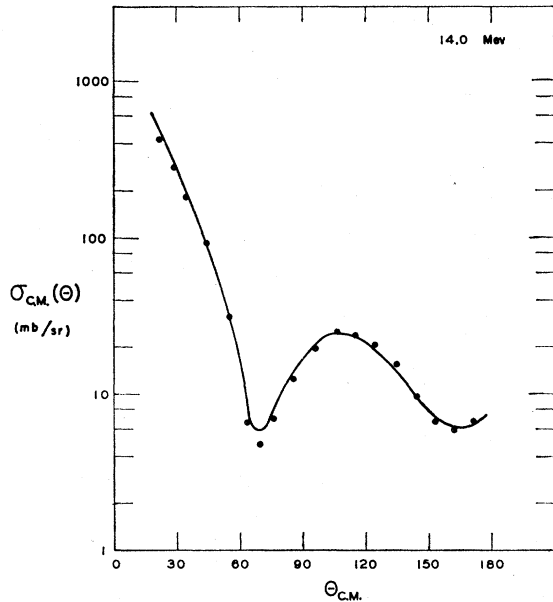


FIG. 16. Optimum fit to the 14-Mev cross-section data incremented by  $-10\%$ . The parameters corresponding to the theoretical curve are:  $R_0=1.20$  f,  $b=0.25$  f,  $\bar{V}=57.3$  Mev,  $W=0$ ,  $W_1=23.1$  Mev,  $a=0.43$  f,  $V_S=-5.7$  Mev,  $W_S=0$ .

Figures 15 and 16 show the optimum fits to the 14-Mev cross-section data incremented by  $+10\%$  and  $-10\%$ , respectively. It is interesting to note that in most cases the optimum fit to the renormalized data

and the optimum fit to the original data are characterized by the same values of  $b$ ,  $W$ , and  $R_0$ . Furthermore, the  $-10\%$  incrementation increased the reaction cross section and in general improved the agreement between theoretical and experimental values.

#### VII. SUMMARY

The present analysis shows that the optical model can account satisfactorily for the elastic scattering of protons from carbon at intermediate energies. The most striking feature of the results is the thin absorptive shell and the small volume absorption which characterizes the potential. Various features of the behavior of the parameters as a function of energy remain to be explained. Finally, the predicted reaction cross section appears generally too low, although the experimental data are not sufficiently precise to warrant drawing a definite conclusion.

#### ACKNOWLEDGMENTS

The authors gratefully acknowledge many valuable discussions with Professors R. Sherr and D. S. Saxon. The authors also wish to thank H. E. Conzett, Y. Nagahara, W. Daehnick and R. Sherr, L. Rosen and L. Stewart, R. Pollock, and T. Yamazaki for graciously providing the detailed results of their experiments prior to publication. Finally, special thanks are due to Lisa Greenstadt, Barbara Ames, and Donald Long for assistance in programming.